Ion irradiation induced direction of collapsed hard-magnetization axis in thin Co films

L. F. S. Azeredo [1,2] J. Geshev [1,*] P. L. Grande [1] and A. M. H. de Andrade [1]

[1]*Instituto de Física, Universidade Federal do Rio Grande do Sul, Porto Alegre, 91501-970 Rio Grande do Sul, Brazil*

[2]*Instituto Federal Sul-rio-grandense, Santana do Livramento, 97574-360 Rio Grande do Sul, Brazil*

(Received 17 December 2022; revised 26 March 2023; accepted 12 April 2023; published 21 April 2023)

A number of polycrystalline films feature distinct sharp peaks in the angular variations of their in-plane major-loop remanent magnetization and coercivity, centered 90° off the easy-axis position, a property referred to as hard-axis collapse. In such systems a striking phenomenon, recoil-curve overshoot (RCO), recoil magnetization branches that lie outside the major loop, was recently reported, resulting in a significantly greater recoil loop area compared with that of the respective major loop. In the present work pieces of polycrystalline magnetron-sputtered Co films were subjected to Ne^+ bombardment in vacuum at different ion fluences in the presence of magnetic field H_{ib} applied along different in-plane directions. Ion irradiation at a certain fluence range results in films with easy-magnetization directions parallel to that of $\mathbf{H_{ib}}$. Moreover, the same holds for posterior sequential irradiations. The films' hard-magnetization axes are always collapsed, accompanied by significant RCO as well. The analysis and interpretation of our data strongly indicate that both hard-axis collapse and RCO result predominantly from a domain splitting when the measurement magnetic field is nearly perpendicular to the grain's easy axis during demagnetization.

DOI: 10.1103/PhysRevB.107.134428

I. INTRODUCTION

Since the pioneering work of Chappert *et al.* [1], which explored the potential for magnetic nanopatterning and showed that the magnetic anisotropy direction can be changed via ion irradiation, the latter has been used to tailor the magnetic properties of thin films and multilayers [2–5]. One of their most important characteristics—the magnetic anisotropy—can be induced by employing a number of techniques [6], including ion beam assisted deposition [7] and/or postgrowth ion irradiation [8]. Also, it is possible, in ferromagnet/antiferromagnet systems, to set or completely reorient the exchange-bias direction by means of ion bombardment [9,10] in the presence of magnetic field H_{ib}.

Recently, an outstanding phenomenon was evidenced in polycrystalline ferromagnetic films: recoil magnetization branches that lie way outside the major hysteresis loop, a phenomenon referred to as recoil-curve overshoot (RCO) [11,12]. As a result, the respective recoil loop's area is significantly greater than that of the major loop. Importantly, the Fe, Co, and Ni films that have shown RCO have also displayed distinct sharp peaks in the angular variations of their in-plane major loops' remanent magnetization M_{RS} and coercivity H_C, centered 90° off the easy-axis position. Such peaks were previously observed in films grown in the presence of a magnetic field and/or after posterior ion bombardment in H_{ib} (see, e.g., Ref. [13] and references therein, corresponding to a series of works by a group from Universität Göttingen). This peculiarity was later referred to as the collapsed hard-magnetization axis [14–16] or hard-axis coercivity rocking [17,18].

The observation of peaks in the angular variations of M_{RS} and H_C after field-assisted ion bombardment in Co/Fe bilayers has been ascribed to a hcp → fcc phase transition, interface mixing, and the formation of intermetallic alloys [19]. In Co/Pt multilayers, the phenomenon has been attributed to ion induced structural changes and modifications of the crystalline field resulting in nonequivalent electronic hybridization between easy and hard axes [20]. In the films that have shown RCO [11,12], phase transitions are discarded given that the phenomenon has been observed in Fe, Co, and Ni films with distinct crystalline structures; it has also been verified that a superposition of cubic and uniaxial anisotropies cannot be responsible for the experimentally observed RCO and angular variations of M_{RS} and H_C.

Despite its simplicity, the model of pairs of exchange-coupled grains with misaligned anisotropy axes proposed by Idigoras *et al.* [14] is able to reproduce qualitatively both the hard-axis collapse and the RCO [11]. Alternatively, these characteristics could be ascribed to a domain splitting when, during demagnetization, the measurement magnetic field **H** is nearly perpendicular to the uniaxial-anisotropy direction [21,22]. Hence, these very peculiar and intriguing features of the magnetic hysteresis certainly warrant further theoretical and experimental investigations which may lead to new applications.

In the present work we demonstrate that an appropriate field-assisted ion bombardment may induce, in a controlled manner, an easy-magnetization direction towards that of $\mathbf{H_{ib}}$ in magnetron-sputtered Co films, with the respective hard-magnetization axes collapsed. A significant RCO is observed as well. Our results point out that these phenomena result, most likely, from a grain's domain splitting when the amplitude of **H**, which is nearly perpendicular to the

*julian@if.ufrgs.br

uniaxial-anisotropy direction, is reduced from a saturation state.

II. EXPERIMENT

Polycrystalline 10-nm-thick Co films, each sandwiched by a pair of seed and protective 18-nm-thick Ta layers, were deposited using dc magnetron sputtering onto naturally oxidized Si(100) substrates at room temperature. The purity of all targets was greater than 99.95%. Each substrate was placed on a holder rotating at 40 rpm, the target-substrate distance was 5.8 inches in a confocal configuration, and the base pressure was below 2×10^{-8} Torr before and 2 mTorr during deposition, at a 20 sccm Ar constant flow. For a majority of the films, in-plane static magnetic field of about 1.5 kOe was applied *in situ* in order to induce uniaxial anisotropy. As-grown samples were subsequently irradiated at room temperature in a 500 High Voltage Engineering Europa linear accelerator at 70 keV with Ne^+ beams at normal incidence in a chamber in 3.5 kOe magnetic field applied along different in-plane orientations. For a constant current density J of 100 nA/cm^2, ion fluences of 1×10^{14}, 1×10^{15}, and 1×10^{16} ions/cm^2 were employed; on the other hand, a fluence value of 1×10^{15} ions/cm^2 was fixed when using different values of J of 25, 50, and 100 nA/cm^2. The strength of the interaction of the irradiation ions with the films, the damage caused, and their range were estimated with SRIM-2013 simulations [23,24].

The structural characterization was performed by x-ray diffraction (XRD) on a Bruker D8 Advance diffractometer at Bragg-Brentano θ-2θ geometry with Cu $K\alpha$ radiation and via Rutherford backscatter spectrometry (RBS) in a 3 MV Tandetron accelerator using a 0.9 MeV beam of incident He ions along the direction normal to the samples' planes with a backscattered ion detector 165° away from the incidence direction.

In-plane magnetization major and recoil hysteresis loops were obtained at room temperature via an EZ9 MicroSense vibrating sample magnetometer. The amplitude values of the maximum magnetic field used here are much higher than the anisotropy field of each of the films, thus avoiding other nonsaturation effects [25–27].

III. RESULTS AND DISCUSSION

Figure 1 shows representative XRD patterns of the as-deposited Co film and of pieces of the same film irradiated in the presence of H_{ib} using either different ion fluences at constant J or different values of J for a fixed ion fluence value. All patterns indicate that the Ta seed layers resulted in highly textured Co surfaces, showing broad peaks at ≈44.5° due to the overlap of the two peaks arising from fcc (111) and hcp (002) planes. It is clear from Fig. 1(b) that, for ion bombardments using a fluence of 1×10^{15} ions/cm^2 and the range of values of J employed here, the value of the latter is irrelevant given that the diffraction patterns are practically identical even for a fourfold difference in J. Thus, the ion beam induced heating effect should certainly be discarded as a possible source for the ion irradiation induced changes in the magnetic properties of the films discussed below.

We also performed x-ray reflectivity (XRR) measurements on several samples. Although, because of the small Co layer

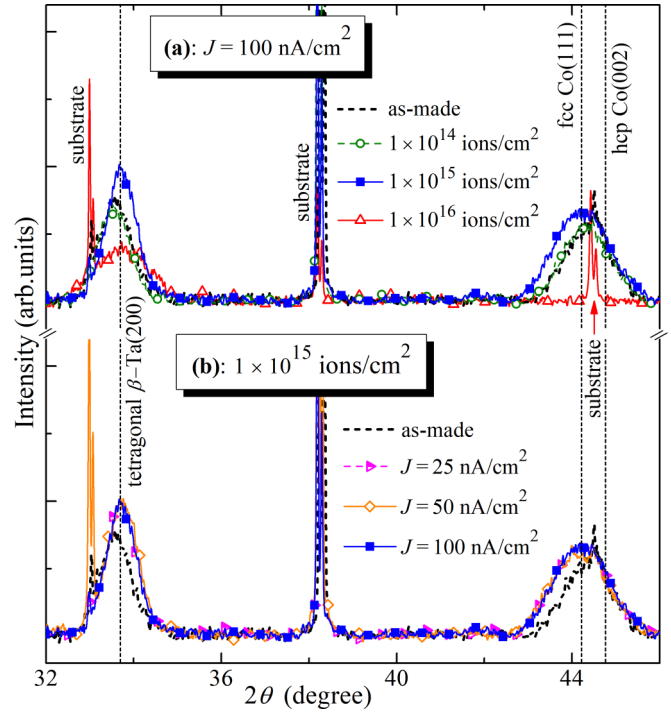

FIG. 1. XRD patterns of the as-deposited Co film as well as of pieces of this film irradiated in magnetic field using (a) different ion fluences at a constant current density and (b) different current densities and fixed ion fluence value.

thickness, the analyses of the experimental and simulated XRR patterns (not shown) are inconclusive, the observed fall in intensity of the Kiessig fringes after Ne irradiation represents a signature of decreased thickness homogeneity and increased interface (and/or film surface) roughness.

Ion bombardment using the lowest fluence value of 1×10^{14} ions/cm^2 did not lead to observable changes in the respective diffraction pattern compared to that of the as-made film. On the other hand, irradiation employing the greatest fluence of 1×10^{16} ions/cm^2 resulted in great changes in the diffraction pattern. A significant reduction of the Ta(002) peak intensity is observed, while no Co peak is detected. This, together with the practically complete loss of magnetic response, attests that this ion bombardment led to severe degrees of damage and of intermixing between the Co and Ta layers, and great structural degradation of the Co layer, completely destroying its ferromagnetism. The XRD pattern of the specimen irradiated with the intermediate fluence of 1×10^{15} ions/cm^2 plotted in Fig. 1(a) shows Co and Ta peaks of higher intensity. Also, the peaks are slightly shifted towards each other, indicating a certain degree of mixture at the Ta/Co and Co/Ta interfaces, most likely responsible for the observed decrease in the magnetic signal.

The above considerations are supported by the collisional damage profiles as a function of the target depth of the Si//Ta/Co/Ta film, calculated with SRIM simulations after 70 keV Ne^+ bombardment [23,24] and plotted in Fig. 2. Although a certain number of Ne ions pass through the deposited layers, others are implanted, predominantly, in the Co layer due to knock-on displacements of Ne^+ from the

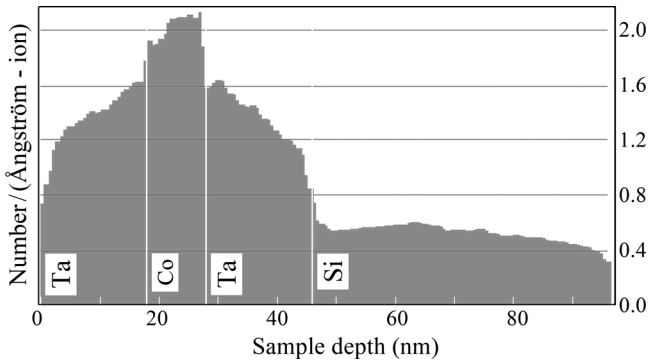

FIG. 2. Collisional damage (the number of target displacements per impinging ion and crossed distance) versus the target depth for 70 keV Ne^+ irradiation into a Si//Ta(18 nm)/Co(10 nm)/Ta(18 nm) film, calculated with a SRIM simulation.

surrounding Ta media, i.e., reflections of Ne^+ at the Ta/Co and Co/Ta interfaces onto the Co film given that the Ta atomic mass is more than 3 time higher than that of Co. The SRIM simulations indicated Ta/Co and Co/Ta interface intermixing is greater at the top Ta/Co interface and that, for the samples irradiated with fluences of 1×10^{14}, 1×10^{15}, and 1×10^{16} ions/cm^2, the relative numbers of Ne atoms implanted in the Co layer are ≈0.01%, 0.1%, and 1%, respectively. The corresponding displacements per atom values estimated here are rather high: 0.23, 2.3, and 23. The implanted Ne associates with vacancies for the fluences used here and can form bubbles at much larger ones [28]. These results imply that the variations in the magnetic properties of our samples reported below are, overall, related to displacements of Co atoms, and the effects of Ne implantation in the ferromagnetic film are of rather minor importance.

RBS analysis gives access to information on the atomic composition as a function of the depth profile, interface mixing, etc. Representative RBS spectra of films bombarded in H_{ib} using two different ion fluence values (the intermediate and highest ones) for $J = 100$ nA/cm^2, together with that of the as-made sample, are plotted in Fig. 3(a). Enhanced overlapping of the Ta peaks and broadening of all Co and Ta peaks with the fluence increase are observed. We performed POWERMEIS simulations (POWERMEIS [29] is a software that calculates, using Monte Carlo methods, the trajectories of all ions in three-dimensional structures) for our RBS spectra [see Fig. 3(b)]. For samples irradiated with Ne^+ using a fluence of 1×10^{15} ions/cm^2 we found that ≈40% of the Co atoms are displaced towards the surrounding Ta layers, creating intermixing at both interfaces. This leads to a reduction of the effective thickness of the magnetic Co layer, in very good agreement with the magnetization data in Figs. 6(a) and 6(c) below. The intermixing is most significant at the top Ta/Co interface, containing ≈75% of the displaced Co atoms, in accordance with the SRIM results as well.

Due to the low amount of Ne and its smaller mass, the presence of implanted Ne could not be identified either from the RBS spectra and the respective POWERMEIS simulations or via the energy dispersive x-ray spectroscopy measurements we also performed (not shown).

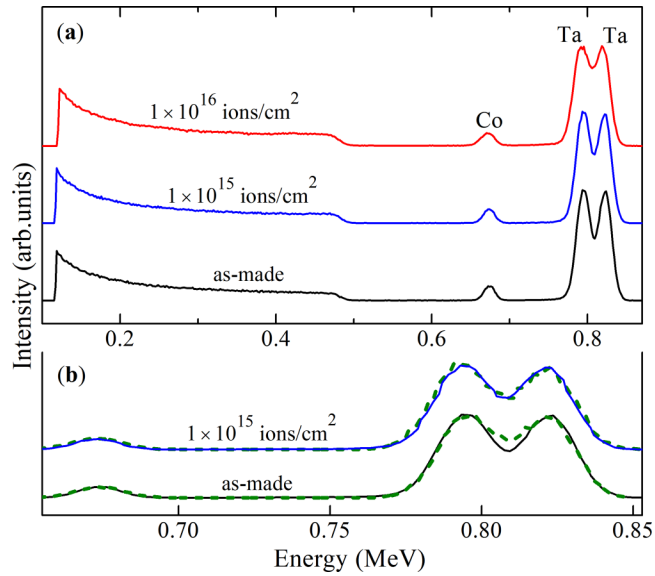

FIG. 3. (a) Experimental Rutherford backscattering spectrometry results for the in-field grown film and for ion-irradiated pieces of this film with in-plane $\mathbf{H_{ib}}$ perpendicular to the deposition induced easy-magnetization direction, using two different fluences and a current density of 100 nA/cm^2. Two of the spectra are displaced vertically for better visualization. (b) POWERMEIS simulations (dashed lines) performed for two of the samples; the solid lines correspond to the measured spectra.

In-plane magnetization data, obtained for the film deposited in magnetic field and irradiated with $\mathbf{H_{ib}}$ parallel to the initial hard-magnetization direction using a fluence of 1×10^{15} ions/cm^2 and $J = 100$ nA/cm^2, are shown in Fig. 4. Here, $\phi_H = 0$ corresponds to measurement magnetic field $\mathbf{H}$ parallel to the irradiation induced easy direction. There are

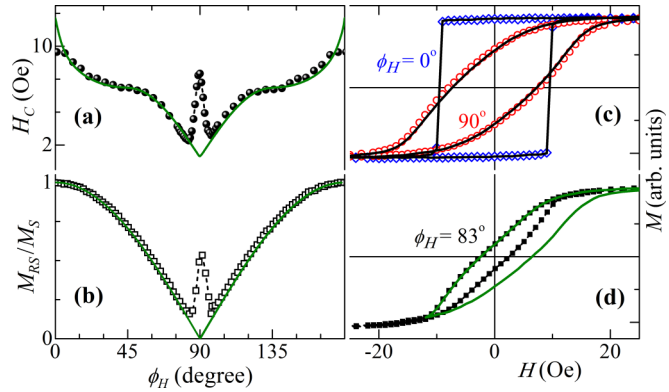

FIG. 4. (a) The major hysteresis loop's coercivity $H_C(\phi_H)$ and (b) remanent magnetization $M_{RS}(\phi_H)$, obtained for the film grown in magnetic field and subsequently ion irradiated with $\mathbf{H_{ib}}$ parallel to the initial hard-magnetization axis using a fluence of 1×10^{15} ions/cm^2 and $J = 100$ nA/cm^2. The solid lines correspond to coherent rotation reversal; M_{RS} is normalized to the saturation magnetization M_S. (c) Major loops (symbols) measured for $\phi_H = 0°$ and 90°; the lines correspond to respective data obtained 5 months earlier. (d) Major (symbols) and recoil (solid line) loops obtained for $\mathbf{H}$ applied near the collapsed hard-magnetization direction.

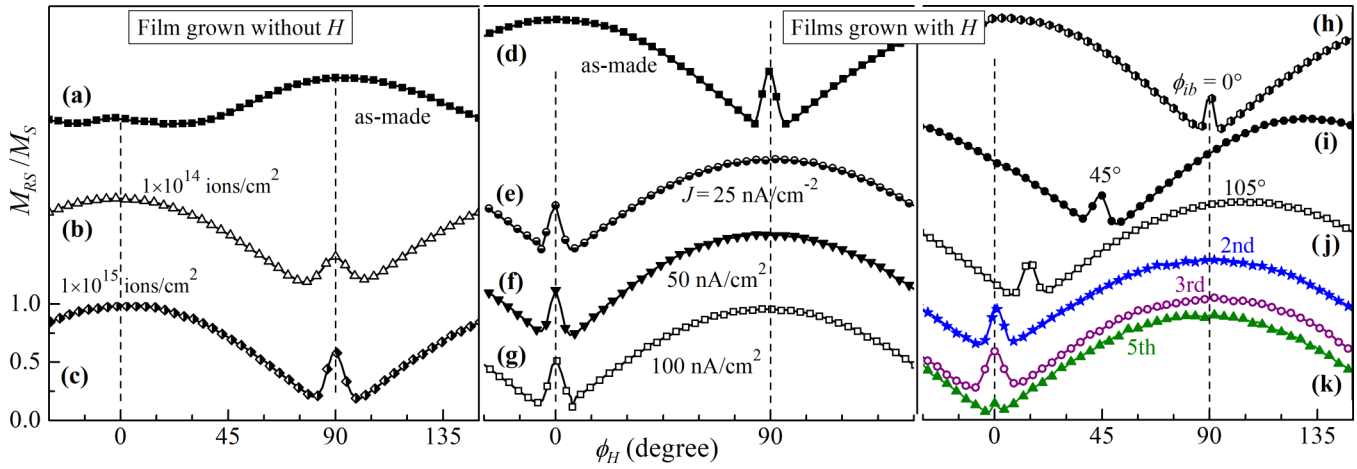

FIG. 5. Angular variations of M_{RS}. (a)–(c) Data for pieces of a film deposited with no purposely applied magnetic field: as made and irradiated with $\mathbf{H_{ib}}$ parallel to the hard-magnetization axis of an as-made film using different ion fluences and the same current density of 100 nA/cm^2. (d)–(k) Results for samples deposited with applied magnetic field: (d)–(g) as made and irradiated with $\mathbf{H_{ib}}$ applied along the in-plane hard axis of the as-made film using an ion fluence of 1×10^{15} ions/cm^2 and different current densities and (g)–(j) irradiated (1×10^{15} ions/cm^2, 100 nA/cm^2) with $\mathbf{H_{ib}}$ along different in-plane directions given by ϕ_{ib}. In (k), the $M_{RS}(\phi_H)$ curves correspond to the sample initially bombarded with $\phi_{ib} = 90°$ [its $M_{RS}(\phi_H)$ is shown in (g)] and subsequently irradiated four more consecutive times with $\mathbf{H_{ib}}$ always perpendicular to the easy axis induced by the preceding bombardment.

well-defined sharp peaks in the angular variations of both H_C and M_{RS}, centered 90° off the easy-axis position, characterizing the hard-axis collapse. The easy- and hard-axis major hysteresis loops are given by the symbols in Fig. 4(c), where the solid lines correspond to data obtained 5 months beforehand. As can be seen, the two sets of loops are virtually identical. The Co layer's oxidation with time was not detected given that the saturation magnetization M_S of this piece of film remained practically the same. The same holds for other measurements we performed, meaning that our films did not show appreciable temporal changes of their magnetization curves' characteristics, i.e., the thermal-drift effect [30]. Also, neither thermal [31] nor athermal [32] training—variations of magnetization hysteresis and/or hysteresis loop characteristics with the number of subsequent field cycles—was observed.

All our as-made and ion-irradiated films that show appreciable collapsed hard axes also present RCO. An example is given in Fig. 4(d), where major and recoil loops traced for ϕ_H corresponding to the minima in both $H_C(\phi_H)$ and $M_{RS}(\phi_H)$ are plotted. The observed recoil-curve overshoot is rather significant, resulting in an approximately twofold loop area increase.

Representative variations of M_{RS} as a function of the measurement field orientation for as-made films deposited with or without applied magnetic field, as well as for specimens of these films irradiated with $\mathbf{H_{ib}}$ applied along different in-plane directions, are given in Fig. 5. Figure 5(a) evidences that the film grown with no purposely applied magnetic field presents rather weak uniaxial anisotropy (only here its easy-axis orientation is denoted by $\phi_H = 90°$) with a collapsed hard axis. Although RCO is observed for this film, it is insignificant. Ion irradiation with fluences of 1×10^{14} and 1×10^{15} ions/cm^2 for $\phi_{ib} = 0°$, i.e., $\mathbf{H_{ib}}$ parallel to the original hard axis, led to radical changes in the anisotropy characteristics, as seen in Figs. 5(b) and 5(c); the data presented in Fig. 4 correspond to those shown in Fig. 5(c). The ion bombardment induced stronger uniaxial anisotropy with the easy axis parallel to $\mathbf{H_{ib}}$ for each fluence value, and with the respective hard axis substantially collapsed. As mentioned above, irradiation with a fluence of 1×10^{16} ions/cm^2 resulted in a complete loss of magnetic response.

Figure 5(d) gives $M_{RS}(\phi_H)$ obtained for the film grown in an applied magnetic field, and Figs. 5(e)–5(g) present the respective angular variations measured after field-assisted ion irradiation with $\phi_{ib} = 0°$ (again, $\mathbf{H_{ib}}$ applied along the initial hard axis) using a constant fluence of 1×10^{15} ions/cm^2 and three different current density values. Clearly, the latter does not influence the outcome given that the three values of $M_{RS}(\phi_H)$ are virtually identical, in total agreement with the XRD results reported above, indicating the irrelevance of the current density value for the anisotropy-axis modifications reported here. In the present case, the strong anisotropy induced during growth is completely eliminated by the field-assisted ion bombardment. The latter results in uniaxial-anisotropy samples with their new easy axes exactly parallel to $\mathbf{H_{ib}}$.

The same holds true for $\mathbf{H_{ib}}$ applied along other in-plane directions during irradiation. Figures 5(g)–5(k) show that, in any case, the easy axis induced through ion bombardment is that of $\mathbf{H_{ib}}$. Note also that the film, which was first irradiated with $\phi_{ib} = 0°$ and, as a result, attained an easy axis along this field direction, had its easy axis completely reoriented along the new field direction when it was subsequently irradiated with $\mathbf{H_{ib}}$ with other orientations.

We also observed that when $\mathbf{H_{ib}}$ is applied along (or close to) the already-set easy-magnetization direction, the bombardment leads to a noticeable decrease in M_{RS}^{HA} (the hard-axis value of M_{RS}/M_S), as exemplified in Fig. 5(h). This is actually expected given that the aforesaid irradiation further aligns the easy axes. Thus, the decrease in M_{RS}^{HA} after bombardment with such an orientation of $\mathbf{H_{ib}}$ confirms the premise that local easy-axis misalignment of the interacting domains is required for the manifestation of both hard-axis collapse and RCO.

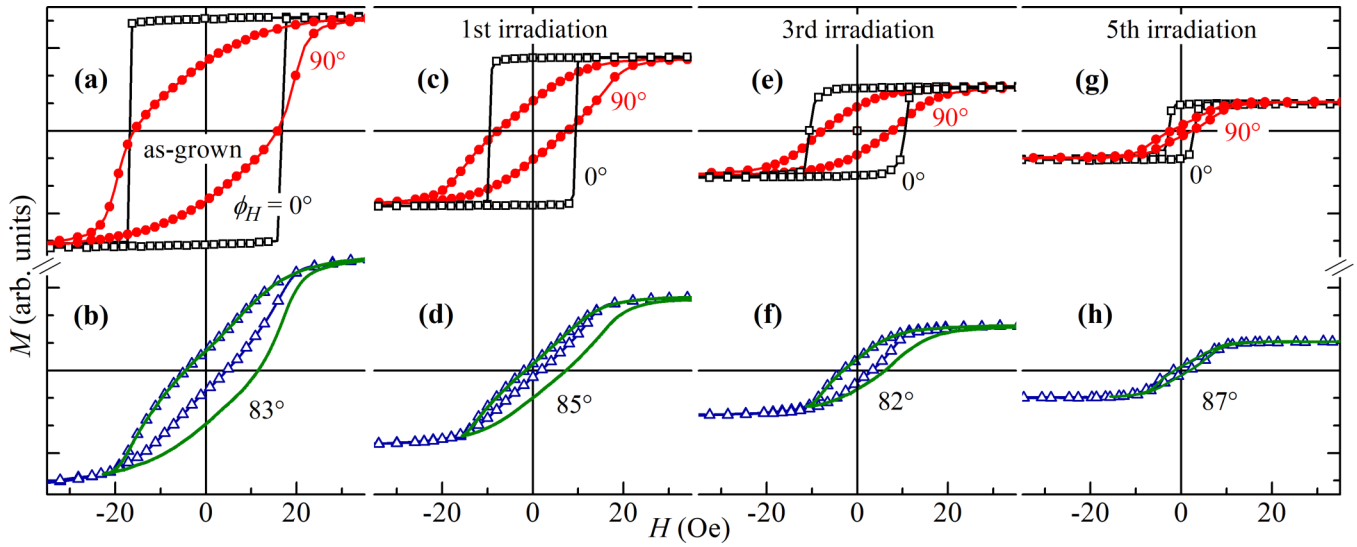

FIG. 6. Major and recoil hysteresis loops measured for a film deposited in an applied magnetic field. (a) and (b) Data obtained for the as-made film. (c)–(h) Loops traced on the same sample after a sequence of ion irradiations with $\mathbf{H_{ib}}$ always perpendicular to the previously induced easy axis using a fluence of 1×10^{15} ions/cm^2 and a current density of 100 nA/cm^2. The top panels show the easy ($\phi_H = 0°$) and hard ($\phi_H = 90°$) axis loops, and the bottom panels give major and recoil loops traced for $\mathbf{H}$ applied in the vicinity of the hard axis.

As mentioned above, all samples presenting significant hard-axis collapse also show recoil-curve overshoot, which is most prominent when ϕ_H corresponds to any of the minima in $H_C(\phi_H)$ and $M_{RS}(\phi_H)$. This is exemplified in Fig. 6, which gives representative major easy- and hard-axis hysteresis loops together with selected major and recoil loops for other $\mathbf{H}$ orientations, obtained for a film grown in an applied magnetic field, subjected to five subsequent ion bombardments with $\mathbf{H_{ib}}$ always perpendicular to the previously induced easy axis. While the loops for $\phi_H = 0°$ display a rectangular shape and those traced for $\phi_H = 90°$ also show significant remanence and coercivity, the major loops measured for $\mathbf{H}$ applied near the collapsed hard-axis direction have rather lower values of M_{RS} and H_C. All those features are characteristics of the hard-axis collapse. The recoil branches for $n \leqslant 4$ plotted in Fig. 6 show significant RCO, with n being the number of the irradiations.

An apparent reduction of H_C and M_S of the ion-irradiated specimen compared to those of the as-grown film is detected in Fig. 6. After the first irradiation, the sample lost approximately half of its coercive field and one third of its original M_S values. The subsequent irradiations led to yet other decreases in M_S without a sizable change in H_C for $n = 2$ and 3. The shrinking of M_S should be related to Co/Ta interface intermixing and knock-on Ne^+ displacements caused by the bombardment, as indicated by the XRD and RBS results. On the other hand, the reduction in H_C with the bombardment could be attributed to both interface roughening and strain relaxation in the Co layer. Importantly, for $n \leqslant 4$ the collapsed hard axis and RCO characteristics remain essentially the same.

XRD patterns of the as-grown Co film and those obtained after the second, fourth, and fifth irradiations with $\mathbf{H_{ib}}$ always perpendicular to the easy axis induced through the previous bombardment are given in Fig. 7(a). Modest and substantial gradual decreases of the Ta and Co peak intensities are seen, respectively. The variation of the average Co grain size D, estimated with Scherrer's formula after the first four irradiations (it is not possible to estimate D for $n = 5$ from the respective XRD pattern), together with that of M_S, is plotted in Fig. 7(b). Both D and M_S decrease steadily with n at very similar rates. Figure 7(c) presents the corresponding (and rather different) variation of M_{RS}^{HA} with n; four of the respective angular variations of M_{RS} are plotted in Figs. 5(g) and 5(k). For uniaxial

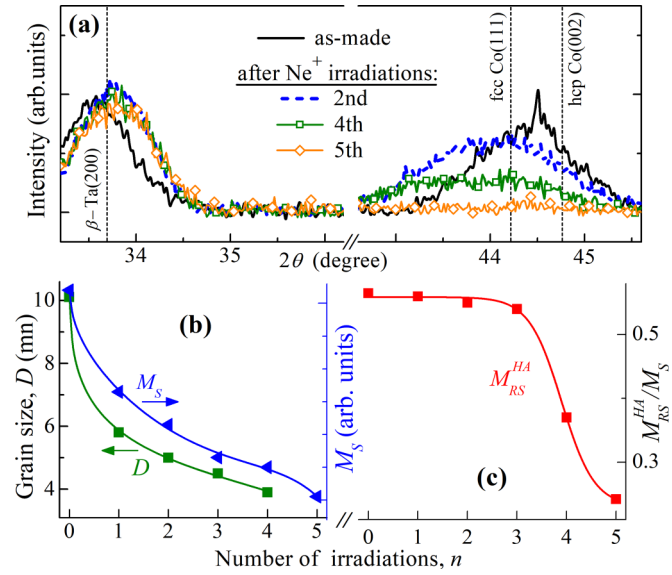

FIG. 7. (a) XRD patterns of the as-grown Co film and of the piece of this film obtained after its second, fourth, and fifth irradiations in H_{ib} (1×10^{15} ions/cm^2 fluence, $J = 100$ nA/cm^2) with $\mathbf{H_{ib}}$ always perpendicular to the easy axis induced by the preceding bombardment. (b) The average grain size and M_S versus the number of bombardments n. (c) The corresponding M_{RS}^{HA} (the hard-axis value of M_{RS}) versus n. The lines are guides to the eye.

anisotropy, the absence of hard-axis collapse corresponds to $M_{RS}^{HA} = 0$ or at least to $M_{RS}(\phi_H)$ having its minimum at $\phi_H = 90^\circ$.

We verified that films irradiated without H_{ib} showed no change in their anisotropy direction and that the reductions in H_C, M_S, and D do not depend on whether H_{ib} is applied or not, pointing out that no Co phase transitions occur due to irradiation. Since $M_{RS}(\phi_H)$ is also independent of the current as discussed above, one can rule out effects coming from the sample's macroscopic heating during the ion bombardment or from the overlap of nuclear or electronic cascades in time. There are other mechanisms that may act during ion bombardment and could lead to the modifications of H_C, M_S, D, and M_{RS}^{HA} and the anisotropy-axis reorientation. One of these mechanisms is the local hyperthermal heating, which is very similar to common magnetic annealing. It serves as an energy source, leading to spin rearrangements which lower the energy of the system. Another relevant mechanism is Ta/Co interface intermixing and interface defect creation by ion bombardment due to the nuclear stopping power of the impinging ions. It depends only on the fluence and works regardless of whether H_{ib} is applied. On the other hand, the field-assisted ion irradiation induced easy-magnetization axis is, most likely, due to the locally transferred energy of the incoming Ne ions. As discussed above, modifications of the magnetic properties coming from Ne implantation, if any, are unsubstantial.

A series of Ta/Co/Ta films [12] grown under the same conditions as those studied here showed an increase of D from $\approx$4 to 17 nm as the Co film thickness increased from 5 to 150 nm, implying that the grains with the largest sizes are located in the last-deposited Co atomic layers. The brisk initial decrease in $D(n)$ seen in Fig. 7 should thus be attributed to the extinction of, above all, these grains after the first irradiation, resulting in a reduction in the effective magnetic Co thickness, which is strongly supported by the very similar rate of decrease of M_S with n. The eradication of the greatest grains, however, does not virtually reflect on M_{RS}^{HA}, which drops substantially for only $n \geqslant 4$.

The earliest model able to mimic the hard-axis collapse considers a magnetic system composed of pairs of exchange-coupled grains with misaligned anisotropy axes [14]. Although this simple model is able to reproduce qualitatively the RCO as well [11], one could question its validity for real polycrystalline magnetic films—it does not seem very realistic to assume that each (supposedly monodomain) grain of these films is exchange coupled to only one (also monodomain) of its neighboring grains.

Simulations formally employing the energy expression of the above model would give the same results if the film is assumed to consist mostly of effectively noninteracting polycrystalline grains, the majority being in a single-domain magnetic state for **H** applied away from the hard axis. During demagnetization from saturation for ϕ_H in the vicinity of 90°, a monodomain would split into two exchange-coupled domains with a slight lateral misalignment [33], in agreement with the results of Hamrle *et al.* [22], who observed domain splitting perpendicular to the collapsed hard axis during demagnetization. This was also predicted through finite-element micromagnetic calculations [34]. The two domains resulting from the splitting are not necessarily identical, and their easy axes may not be exactly symmetrical with respect to that of **H**. The recently observed negative interaction plots resulting from ferromagnetic coupling and hysteretic recoil loops with positive recoil fields in Co films with collapsed hard axes [12] were successfully reproduced by this model.

The expression "effectively noninteracting" used above refers, for the principal part of Co grains, to the plausible zero net effect of interactions produced by neighbors owing to the local spherical symmetry. The fitting curves for $M_{RS}(\phi_H)$ and $H_C(\phi_H)$ in Figs. 4(a) and 4(b) calculated with the single-domain noninteraction coherent rotation model [35] clearly show that, at least for two thirds of the angular range, such a rotation is the dominant magnetization reversal mechanism already observed for Co films with different thicknesses [11,12] presenting hard-axis collapse or RCO.

The $M_S(n)$ variation in Fig. 7(c) points out that more than half of the amount of magnetic Co has been extinguished after the third ion irradiation. The almost identical rate of decrease of $D(n)$ denotes that this is due to the eradication of the larger Co grains. Nevertheless, the quantity that identifies the hard-axis collapse, namely, M_{RS}^{HA}, diminished less than 5% after the third bombardment. Given that, for each n, M_{RS}^{HA} is normalized to the respective M_S value, its virtual constancy indicates that the relative amount of Co contributing to the collapse has practically the same weight regardless of the Co grain sizes before and after the first three ion irradiations. The consequent bombardments led to a further decrease in the amount of magnetic Co with yet smaller grain size, lowering the possibility for domain splitting and causing the significant drop in M_{RS}^{HA} and nonobservance of RCO [see Fig. 6(h)]. All these results agree with the predominance of the domain-splitting hypothesis. On the contrary, in the framework of the model of pairs of exchange-coupled single-domain grains [14], the bigger bi- or multidomain grains do not contribute to either hard-axis collapse or RCO, and consequently, their eradication would result in a significant increase in M_{RS}^{HA}/M_S caused by the more than twofold decrease in M_S instead of the modest decline actually observed.

Further corroboration of the viability of the conjecture for domain splitting comes from results for the interaction effects recently estimated in slightly thicker Co films [12]. For field orientations where coherent magnetization reversal is predominant, the interaction plots are typical of polycrystalline films with weakly interacting ferromagnetic grains. However, in the region of ϕ_H which characterizes a collapsed hard axis and RCO and where scissorslike reversible rotations take place, the intensity of the interaction plots increases substantially, most likely due to the emergence of intragrain coupling between twin domains resulting from the monodomain splitting as H is swept down to zero.

IV. SUMMARY AND CONCLUSIONS

In summary, we demonstrated that appropriate ion bombardment with magnetic field applied in the plane of magnetron-sputtered Co films induces well-defined uniaxial anisotropy with an easy-magnetization direction parallel to that of $\mathbf{H_{ib}}$. Up to five sequential ion irradiations, despite

the decreasing average Co grain size and the effective thickness of the magnetic Co layer, induced anisotropy with the easy axis always parallel to $\mathbf{H_{ib}}$. Importantly, the films' hard-magnetization axes always collapsed, accompanied by significant recoil-curve overshoot. None of the irradiated films showed appreciable thermal drift or training effects. We pointed out the sources likely to supply energy for spin rearrangement and lead to the easy-axis modifications of ion-irradiated films.

Our results strongly indicate that the puzzling hard-axis collapse and RCO phenomena result essentially from grains in a monodomain state which magnetizations split into pairs of exchange-coupled domains with a slight local easy-axis misalignment when the measurement magnetic field, which is nearly perpendicular to the uniaxial-anisotropy direction, is reduced from a saturation state.

ACKNOWLEDGMENT

This work was supported by the Brazilian agencies CNPq (Grant No. 406009/2021-0), FAPERGS (Grant No. 21/2551-0002019-9), and CAPES.

[1] C. Chappert, H. Bernas, J. Ferre, V. Kottler, J.-P. Jamet, Y. Chen, E. Cambril, T. Devolder, F. Rousseaux, V. Mathet, and H. Launois, Science **280**, 1919 (1998).
[2] J. Fassbender, D. Ravelosona, and Y. Samson, J. Phys. D **37**, R179 (2004).
[3] J. Fassbender and J. McCord, J. Magn. Magn. Mater. **320**, 579 (2008).
[4] A. V. Krasheninnikov and K. Nordlund, J. Appl. Phys. **107**, 071301 (2010).
[5] A. Talapatra, U. Gajera, S. Prasad P, J. A. Chelvane, and J. R. Mohanty, ACS Appl. Mater. Interfaces **14**, 50318 (2022).
[6] K. Itoh, J. Magn. Magn. Mater. **95**, 237 (1991).
[7] W. A. Lewis, H. Saffari, M. Farle, E. Kay, and S. B. Hagstrom, Mater. Res. Soc. Symp. Proc. **268**, 161 (1992); M. Farle, H. Saffari, W. A. Lewis, E. Eay, and S. B. Hagstrom, IEEE Trans. Magn. **28**, 2940 (1992).
[8] M. Neubauer, N. Reinecke, M. Uhrmacher, K. P. Lieb, M. Münzenberg, and W. Felsch, Nucl. Instrum. Methods Phys. Res. Sect. B **139**, 332 (1998).
[9] A. Ehresmann, D. Engel, T. Weis, A. Schindler, D. Junk, J. Schmalhorst, V. Höink, M. D. Sacher, and G. Reiss, Phys. Status Solidi B **243**, 29 (2006).
[10] D. Schafer, J. Geshev, S. Nicolodi, L. G. Pereira, J. E. Schmidt, and P. L. Grande, Appl. Phys. Lett. **93**, 176101 (2008).
[11] J. Geshev, W. J. S. Garcia, V. Z. C. Paes, L. F. S. Azeredo, L. S. Dorneles, and A. M. H. de Andrade, Phys. Rev. B **104**, 054436 (2021).
[12] J. Geshev and A. M. H. de Andrade, J. Magn. Magn. Mater. **560**, 169573 (2022).
[13] K. P. Leib, K. Zhang, G. A. Müller, R. Gupta, and P. Schaaf, Hyperfine Interact. **160**, 39 (2005).
[14] O. Idigoras, A. K. Suszka, P. Vavassori, P. Landeros, J. M. Porro, and A. Berger, Phys. Rev. B **84**, 132403 (2011).
[15] O. Idigoras, A. K. Suszka, P. Vavassori, B. Obry, B. Hillebrands, P. Landeros, and A. Berger, J. Appl. Phys. **115**, 083912 (2014).
[16] M. Sedrpooshan, H. Ahmadvand, D. L. González, and S. van Dijken, Phys. Rev. B **98**, 214444 (2018).
[17] C. Mathieu, V. R. Inturi, and M. J. Hadley, IEEE Trans. Magn. **44**, 431 (2008).
[18] V. Inturi, H. Yin, M. Kief, M. Hadley, and C. Mathieu, IEEE Trans. Magn. **48**, 1718 (2012).
[19] K. Zhang, R. Gupta, G. A. Müller, P. Schaaf, and K. P. Lieb, Appl. Phys. Lett. **84**, 3915 (2004).
[20] G. S. Chang, A. Moewes, S. H. Kim, J. Lee, K. Jeong, C. N. Whang, D. H. Kim, and S.-C. Shin, Appl. Phys. Lett. **88**, 092504 (2006).
[21] J. Nowak and E. Szibel, IEEE Trans. Magn. **20**, 2105 (1984).
[22] J. Hamrle, S. Blomeier, O. Gaier, B. Hillebrands, R. Schäfer, and M. Jourdan, J. Appl. Phys. **100**, 103904 (2006).
[23] SRIM, http://www.srim.org.
[24] J. F. Ziegler, M. D. Ziegler, and J. P. Biersack, Nucl. Instrum. Methods Phys. Res. Sect. B **268**, 1818 (2010).
[25] J. Geshev, L. G. Pereira, and V. Skumryev, Phys. Rev. Lett. **100**, 039701 (2008).
[26] J. Geshev, J. Phys.: Condens. Matter **21**, 078001 (2009).
[27] A. Harres, M. Mikhov, V. Skumryev, A. M. H. de Andrade, J. E. Schmidt, and J. Geshev, J. Magn. Magn. Mater. **402**, 76 (2016).
[28] S. Peripolli, E. Oliviero, P. F. P. Fichtner, M. A. Z. Vasconcellos, and L. Amaral, Nucl. Instrum. Methods Phys. Res. Sect. B **242**, 494 (2006).
[29] M. A. Sortica, P. L. Grande, G. Machado, and L. Miotti, J. Appl. Phys. **106**, 114320 (2009); POWERMEIS, http://tars.if.ufrgs.br.
[30] A. Ehresmann, D. Junk, D. Engel, A. Paetzold, and K. Röll, J. Phys. D **38**, 801 (2005).
[31] A. Hoffmann, Phys. Rev. Lett. **93**, 097203 (2004)
[32] A. Harres and J. Geshev, J. Phys.: Condens. Matter **23**, 216003 (2011).
[33] F. Scheurer, R. Allenspach, P. Xhonneux, and E. Courtens, Phys. Rev. B **48**, 9890 (1993).
[34] W. Rave, K. Fabian, and A. Hubert, J. Magn. Magn. Mater. **190**, 332 (1998).
[35] E. C. Stoner and E. P. Wohlfarth, Philos. Trans. R. Soc. London Ser. A **240**, 599 (1948).